https://doi.org/10.5194/egusphere-2026-1341
Preprint. Discussion started: 13 April 2026

Combining different views on internal climate variability of temperature over Europe

Herijaona Hani-Roge Hundilida Randriatsara[1], Eva Holtanová[1], Jiří Mikšovský[1]

[1] Department of Atmospheric Physics, Faculty of Mathematics and Physics, Charles University, Prague, V Holešovičkách 2, 18000, Prague 8, Czech Republic

Correspondence to: Herijaona Hani-Roge Hundilida Randriatsara (hundilida.randriatsara@matfyz.cuni.cz)

Abstract. Internal climate variability (ICV) estimates provide a useful benchmark for assessing climate model performance and the emergence of anthropogenically forced climate change. This study aims to quantify the magnitude of ICV using different types of data, representing both Earth System Model simulations and observation-based datasets. We focus on seasonal mean near surface air temperature over Europe utilizing different methodological approaches: assessment of variability inferred from pre-industrial control simulations, spread of a single-model initial-condition large ensemble, separation of uncertainty sources in CMIP6 transient simulations, and forcing attribution in observed time series. Across all methods and datasets, we found that ICV estimates decrease during the seasonal course from winter to autumn and spatially from north-eastern to south-western Europe. By comparing the results of the historical and scenario simulations of the large ensemble and selected CMIP6 models, we conclude that European ICV generally decreases under anthropogenically forced climate change. Moreover, our study suggests that applying ICV estimates as a benchmark for assessing regional climate simulations over Europe should be approached with caution. The estimate based on the pre-industrial control simulations offers an advantage since the simulations are not influenced by external forcings and their ensemble mean estimate encompasses the range of the other methods. When the focus is on future climate simulations, estimates from scenario simulations should be used, as they already account for the influence of anthropogenic forcings on ICV. Regarding ICV estimates from observational data, their advantage lies in accounting for true climate history, free of modelling uncertainty. Historical simulations also account for historical climate change and yield ICV estimates comparable to those from observational data.

1 Introduction

Partitioning the uncertainty of climate change projections into three main sources, known as model uncertainty, scenario uncertainty, and internal climate variability (ICV) uncertainty, is helpful not only for scientific interpretation and improving climate models but also for science communication (Knutti and Sedláček, 2012; Abramowitz et al., 2019). Model uncertainty, also called climate response uncertainty, is attributed to structural differences between models and how they respond to external forcing. This arises from different choices made by individual modeling centers while constructing and tuning their models. In principle, this uncertainty is reducible since the differences between models and between models and observations are

https://doi.org/10.5194/egusphere-2026-1341
Preprint. Discussion started: 13 April 2026

artifacts of model imperfection (Abramowitz et al., 2019; Lehner et al., 2020; Merrifield et al., 2023). Moreover, uncertainties in the observational data can also play a role (i.e., the data used as 'observations' are rarely a perfect representation of the real climate system). Scenario uncertainty or radiative forcing uncertainty arises from a lack of knowledge of future radiative forcing, which is primarily driven by unpredictable socio-economic factors (Hawkins and Sutton, 2009; Lehner et al., 2020). It is possible to quantify scenario uncertainty using a consistent, sufficiently large set of models run under different socio-economic scenarios. Unlike Model uncertainty, Scenario uncertainty is irreducible since the probability of future evolution of anthropogenic factors is currently unknown (Gosling et al., 2012; Booth et al., 2013; Lehner et al., 2020; Deser and Phillips, 2023). And lastly, the uncertainty connected to the ICV exists due to the chaotic nature of the climate system. Thus, this uncertainty is inherently irreducible (Deser et al., 2010 and 2014; Kay et al., 2015; Olonscheck and Notz, 2017; Jain et al., 2023).

Focusing mainly on the ICV, it is defined as a natural variability within the climate system that occurs without external forcing involvement (Deser et al., 2010 and 2014; Thompson et al., 2015; Chen et al., 2021). Uncertainty associated with the ICV is one of the major sources of climate change projection uncertainties, due to the unpredictability of the evolving processes and interactions within the climate system itself (Deser et al., 2010 and 2020; Schwarzwald and Lenssen, 2022; Blanusa et al., 2023; Lehner and Deser, 2025). The climate system is known to be a nonlinear dynamical system (Dethloff et al., 2007). The interactions between its components involve energy, momentum, and mass transfers, and feedbacks across multi-spatial and temporal scales (Palmer, 1999; McWilliams, 2007; IPCC, 2021a). Nonlinearity and the resulting chaoticity in the system mean that just a small perturbation in the initial conditions can expand exponentially, leading to uncoupling of originally close climate system trajectories. For this reason, the climate system exhibits sensitive dependence on initial conditions, making its internal variability unpredictable beyond a certain time horizon (Lorenz, 1963; Ghil and Lucarini, 2020). This sensitive dependence, together with models' imperfections, limits the reliability of projections after the initial condition information has been lost, typically a few years (or even less than a year) for the climate projections (Lorenz, 1963 and 1996) and less than 10 days for weather prediction (Krishnamurthy, 2019). This eventually affects the climate projection outcome and contributes to the irreducibility of ICV uncertainty. Moreover, the ICV is perceived through some modes of variability with intrinsic randomness (such as El Niño Southern Oscillation, Atlantic Multidecadal Variability, Pacific Decadal Variability, etc.), which arise from the system's dynamics (Collins et al., 2010; Deser et al., 2010; IPCC, 2021b). They might evolve unpredictably to some extent, and their future phase and amplitude are intrinsically uncertain (Ghil and Lucarini, 2020; Jain et al., 2023).

The Intergovernmental Panel on Climate Change Sixth Assessment Report (IPCC AR6) emphasized that the evidence for human influence on recent climate change reported from IPCC AR2 to AR5 has become stronger during recent decades (IPCC, 2021c). This human influence has been impacting the whole climate system. It has been attributed to, for example, increasing greenhouse gas concentrations, changes in land use, and emissions of human-made aerosols (e.g., sulfates, black carbon). In sum, these effects have led to positive radiative forcing, resulting in increased observed warming (IPCC, 2021c). The anthropogenic influence resulting in forced climate change not only modulates the mean climate but also the characteristics of ICV itself and the overall climatic variability and extremes (Deser et al., 2010; LaJoie and DelSole, 2016; Rodgers et al., 2021;

https://doi.org/10.5194/egusphere-2026-1341
Preprint. Discussion started: 13 April 2026

Deser and Phillips, 2023). One among other examples, a recent study of Beobide-Arsuaga et al. (2025) found out that forced changes in internal variability will intensify summer heatwaves over central and northern Europe, while they are projected to weaken southern European summer heatwaves. Many studies illustrate how external forcing might change internal variability characteristics (Deser et al., 2010; LaJoie and DelSole, 2016; Rodgers et al., 2021; Deser and Phillips, 2023). Thus, to more accurately assess climate change on various temporal and spatial scales, it is essential to evaluate the ICV and its interaction with both natural and anthropogenic influences. That is included in the goal of this study to consider these two influences and to estimate ICV as a benchmark for detecting forced climate change.

Previous studies have assessed ICV using various approaches and data types. For example, Hawkins and Sutton (2009) assessed ICV by using historical and scenario simulations from global climate models. They fit a fourth-order polynomial to the simulated time series and assess the ICV magnitude from the fit residuals. This method has been applied for partitioning model uncertainty in many other studies using climate model datasets (Hawkins and Sutton, 2011; Yip et al., 2011; Lehner et al., 2020; Snyder et al., 2024; Evin et al., 2024). Another widely used approach to ICV assessment involves pre-industrial control simulations (Olonscheck and Notz, 2017; Menary et al., 2018; Rehfeld et al., 2020; Van Achter et al., 2020; Sippel et al., 2021; Mann et al., 2022; Zappa et al., 2021). These provide long time series spanning from hundreds to thousands of years and are run under fixed external forcings at pre-industrial levels (typically year 1850, Eyring et al., 2016). Thus, there is no influence of changes in external forcings, and any variability in the simulation comes solely from internal processes of the climate system. Further, Single-Model Initial-condition Large Ensembles (SMILEs) simulations are considered robust tools for assessing ICV since they are created using a single climate model run under the same external forcing but with slightly different initial conditions, which is designed to isolate ICV from other uncertainties (Lehner et al., 2020; Deser et al., 2020; Maher et al., 2021). Depending on the computational capacity of each modeling center, a SMILE typically consists of 30 to 100 members. Many studies have successfully used one or more SMILEs to examine ICV behavior, including Kay et al. (2015), Martel et al. (2018), Maher et al. (2020), Lehner et al. (2020), and Shen et al. (2024), among others.

Given that each of the previously mentioned methods and datasets plays a valuable role in assessing ICV, this study combines, for the first time, several approaches and datasets (including observational data) to compare and assess ICV magnitude from diverse perspectives. This is done to provide a useful benchmark for eventually evaluating the performance of global and regional climate models over Europe. We focus on the annual and seasonal means of near-surface air temperature. In general, four different approaches based on different datasets are used in this study to assess the ICV estimates: (1) pre-industrial control simulations of CMIP6 (Coupled Model Intercomparison Project Phase 6) models (noted as Pidata), (2) historical and scenario simulations from CMIP6, (3) SMILE simulations from the MPI-ESM model, and (4) observational data.

https://doi.org/10.5194/egusphere-2026-1341
Preprint. Discussion started: 13 April 2026

2 Study area

The study area encompasses the European region, divided into four subdomains, as shown in Figure 1. Three of the four subregions were defined based on the updated IPCC WGI reference regions (Iturbide et al., 2020) and are noted as NEU (Northern Europe), WCE (Western and Central Europe), and MED (Mediterranean). The last subregion, denoted CEU (Central Europe) and bordered by the dashed rectangle in Fig. 1, is of interest for climate change scenarios in the Czech Republic and surrounding regions, especially for convection-permitting regional climate model simulations that focus on this region. The ICV estimates developed in the current study will be further used as a benchmark for assessing model performance and future climate change projections over this area (Randriatsara et al., 2026a).

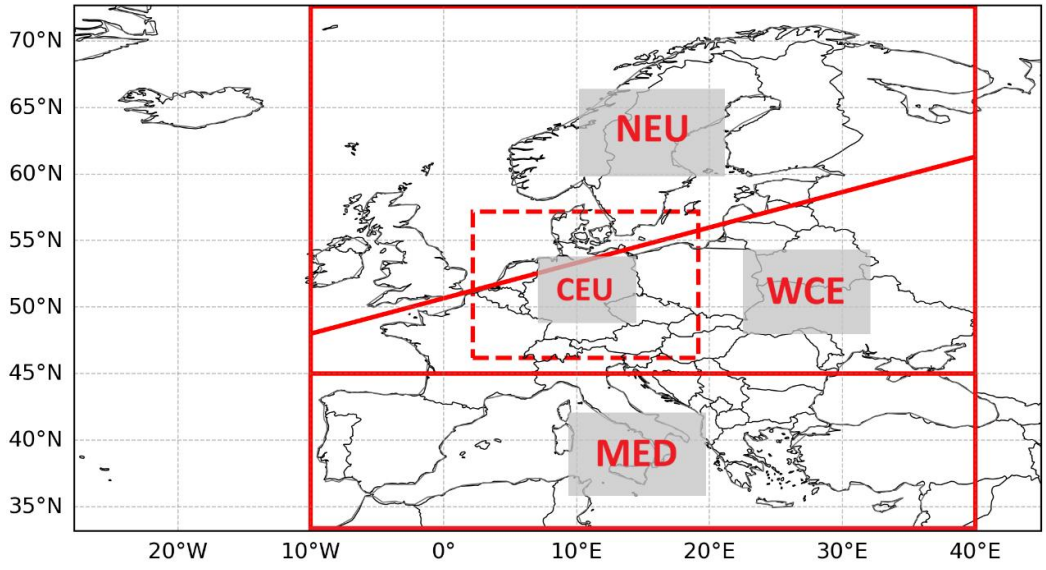

Figure 1: Subregions used in this study. The subregions within the red solid contours, from north to south, are the NEU, WCE, and MED domains, and the dashed red contour pertains to the CEU domain.

3 Methods and data

For all four different types of datasets and approaches, ICV estimates were computed from time series of seasonal and annual mean near-surface air temperature.

3.1 Pidata: Pre-industrial control simulations

The Pidata in the present study are chosen from 15 CMIP6 models listed in Table 1 (Eyring et al., 2016). The simulations were run under 1850 forcings and are 500 years long. The 15 models were selected because they share the same target period, from 1850 to 2349. For the case of Pidata, the analysis of ICV was done through the computation of standard deviation (Olonscheck

https://doi.org/10.5194/egusphere-2026-1341
Preprint. Discussion started: 13 April 2026

and Notz, 2017). First, the simulated temperature time series were linearly detrended, so that the effect of drift would not contaminate the estimate of ICV (Gupta et al., 2013). Then, we calculated the standard deviation for each model and the ensemble mean of the standard deviations (noted as ENSMEAN). Afterward, we regridded all the data onto a common 1-degree grid (Longitude and Latitude). This is done to retain as much of the information from their original grids as possible. The 1-degree resolution was chosen because many models have resolutions around 1 degree, making it a middle ground. Moreover, comparisons between the original and regridded grids show almost no difference (Fig. S1).

3.2 Historical and scenario CMIP6 simulations: Hawkins and Sutton (2009) method

The same 15 CMIP6 models as in the case of Pidata were used, focusing on their historical simulations for the period 1971-2014 and runs under SSP5-8.5 (Eyring et al., 2016) for the period 2014-2100. They were employed to assess the magnitudes of ICV under the existence of external forcings. We chose the socio-economic scenario SSP5-8.5 because it represents the higher end of the available scenarios in terms of anthropogenic influence on the climate system (ref. to SSPs). So the potential influence of external forcing on ICV will be easier to detect than in lower-emission scenarios. Here, the ICV was estimated for three time periods: Historical (1971-2000), future (2070-2099), and the whole (1971-2100). We use the method of Hawkins and Sutton (2009) (further noted as HS09). The ICV for each model is defined as the variance of the residuals from the fits of ordinary least squares with a fourth-order polynomial. Similar to the Pidata analysis, the ICV estimates were regridded to a common 1-degree resolution. The results based on the Hawkins and Sutton (2009) method using the CMIP6 simulations will be further denoted as HS09 results, and the ENSMEAN will refer to the multimodel mean value.

3.3 SMILE data from the MPI-ESM model with 100 members

The SMILE simulations of the MPI-ESM model with 100 members (Maher et al. 2019) are, to our knowledge, the largest single-model ensemble currently available. It was run with the horizontal resolution of 1.875 degrees (Longitude x Latitude), and we chose scenario simulations under RCP8.5. The assessment of ICV estimate based on this SMILE was done as follows. We calculated the anomaly relative to the long-term mean for each member in both the historical (1971-2000) and scenario (2070-2099) periods. Then, we subtracted each anomaly from its ensemble mean (or the forced signal) to remove the effects of the forced distribution shift. So, the ICV is the spread of these differences computed as the standard deviation across all 100 members. The same procedure was used in previous papers (e.g., Martel et al., 2018; Maher et al., 2020; Lehner et al., 2020). Before calculating the standard deviation, each member was regridded to 1-degree resolution.

3.4 Observational data

We use three observational-based temperature datasets specified below (Table 2) and apply a regression model to remove components attributable to external forcings, leaving only ICV-related variability in the regression residuals. For each of the three observational data, the temperature time series at individual grid points for the period 1901-2010 were processed using multiple linear regression, with predictors pertaining to greenhouse gas concentration, volcanic aerosol optical depth, and solar

https://doi.org/10.5194/egusphere-2026-1341
Preprint. Discussion started: 13 April 2026

activity, as described in Mikšovský et al. (2016). The results from regression-based removal of components related to external climate forcings will be further denoted as observational results.

Table 1: Global climate models used for Pidata and CMIP6

Name	Modelling center	Horizontal Resolution
BCC-CSM2-MR	Beijing Climate Center Climate System Model	~125 km
CMCC-CM2-SR5	Fondazione Centro Euro-Mediterraneo sui Cambiamenti Climatici (CMCC), Lecce, Italy	~139 km
CMCC-ESM2	Fondazione Centro Euro-Mediterraneo sui Cambiamenti Climatici (CMCC), Lecce, Italy	~155 km
CNRM-CM6-1	Centre National de Recherches Meteorologiques (CNRM) and Centre Europeen de Recherche et de Formation Avancee en Calcul Scientifique (CERFACS), Toulouse, France	~155 km
CNRM-ESM2-1	Centre National de Recherches Meteorologiques (CNRM) and Centre Europeen de Recherche et de Formation Avancee en Calcul Scientifique (CERFACS), Toulouse, France	~156 km
EC-Earth3-CC	EC-Earth consortium, Rossby Center, Swedish Meteorological and Hydrological Institute/SMHI, Norrköping, Sweden	~78 km
EC-Earth3-Veg	EC-Earth consortium, Rossby Center, Swedish Meteorological and Hydrological Institute/SMHI, Norrkoping, Sweden	~78 km
HadGEM3-GC31-LL	Met Office Hadley Centre, UK	~ 208 km
HadGEM3-GC31-MM	Met Office Hadley Centre, UK	~ 93 km
INM-CM4-8	Institute for Numerical Mathematics (INM), Russian Academy of Science, Moscow, Russia	~ 222 km
IPSL-CM6A-LR	Institut Pierre Simon Laplace (IPSL), Paris, France	~ 278 km
MIROC-ES2L	Japan Agency for Marine-Earth Science and Technology (JAMSTEC), Kanagawa, Japan, Atmosphere and Ocean Research Institute (AORI), The University of	~ 311 km
MPI-ESM1-2-HR	Max Planck Institute for Meteorology, Germany	~ 104 km
MPI-ESM1-2-LR	Max Planck Institute for Meteorology, Germany	~ 208 km
MRI-ESM2-0	Meteorological Research Institute, Japan	~ 125 km

https://doi.org/10.5194/egusphere-2026-1341
Preprint. Discussion started: 13 April 2026

Table 2: Observational datasets.

Dataset name	Acronym	Horizontal resolution	Reference
Goddard Institute for Space Studies Surface Temperature Analysis	GISTEMP	2 x 2 degree	Lenssen, N. et al. (2024)
Berkeley Earth Surface Temperature	Berkeley	1 x 1 degree	Rohde and Hausfather (2020)
NOAA–CIRES–DOE Twentieth Century Reanalysis, Version 3 (20CRv3)	20CR	1 x 1 degree	Slivinski et al. (2019)

4 Methods and data

4.1 Spatial distribution of ICV estimates

In general, the spatial distributions of the ICV estimates for both annual and seasonal timescales show a similar pattern between all methods and time periods (Figs. 2-3). Except during the summer season, the highest values are in most cases found over the north-eastern part of the study domain. Looking into details, the annual temperature exhibits weaker ICV estimates between 0.2 and 1.0 °C (Figs. 2c and 3). The DJF season shows the highest values, exceeding 2 °C (Figs. 2a and 3). The largest values, exceeding 3.0 °C, are found over north-eastern Europe, as shown by Pidata (Fig. 3z). In MAM, the ICV values are lower than in DJF, ranging from 0.3 °C to 2.0 °C (Fig. 2b and 3). For the case of JJA, the ICV estimates range from 0.2 °C to 1.7 °C, but the higher estimates shift southward and cover the latitudes between 40°N and 56°N (Fig. 3). Except for the observational data, the larger ICV estimates are found only over the eastern part of these latitudes (Fig. 2d). The SON pattern is similar to DJF and MAM but with smaller ICV estimates between 0.3 °C and 1.7 °C (Figs. 2e and 3). Overall, ICV estimates across the European region decrease from north-east to south-west on both annual and seasonal timescales, except during JJA, when the highest ICV magnitudes move southward. The annual analysis yields smaller ICV estimates than the seasonal analyses, while DJF shows the largest ICV magnitudes across all seasons. Pidata provides the highest ICV estimates among all the approaches and timescales, except during JJA. GISTEMP shows lower ICV estimates than the other results, while Berkeley and 20CR display comparable ICV estimates in most cases.

Additionally, the annual ICV estimates for each of the 15 individual CMIP6 models (Pidata, historical, and scenario simulations) are shown in the Supplement to provide inter-model comparison (Figs. S2-S5). Pidata display the highest ICV estimates for each individual model (Fig. S2), whereas the scenario simulations show the lowest values for each model (Fig. S4). BCC-CSM2-MR model simulates the highest ICV magnitude among all other models in all the approaches, while EC-Earth3-CC and EC-Earth3-Veg models show a remarkably high ICV in Pidata (Fig. S2), especially over the extreme north of the study area. Unlike in Pidata, in which the higher values decrease from the north-east to the south for all models (Fig. S2),

https://doi.org/10.5194/egusphere-2026-1341
Preprint. Discussion started: 13 April 2026

some models in the historical and scenario simulations display different patterns. For instance, CMCC-EMS2, CNRM-ESM2-1, EC-Earth-Veg, and HadGEM3-GC-MM show that the higher ICV estimates are located over the central part of the study domain (Figs. S3-S5). There are also some models that display different patterns depending on each period. This is the case for HadGEM3-GC-LL, INM-CM4-8, and MRI-ESM2, in which higher ICV estimates are observed across different locations. For example, the higher values for the case of HadGEM3-GC-LL are located in central northern Europe during the historical simulation (1971-2000) (Fig. S3), while they shift to the central and north-east parts during the future (2070-2099) (Fig. S4) and the full simulation period (1971-2100) (Fig. S5) periods, respectively. For the case of INM-CM4-8, the higher values are located over the central part during the historical period (Fig. S3), while they are found over the northern part during the future (Fig. S4) and the whole time (Fig. S5) periods. Moreover, the MRI-ESM2 model displays higher ICV estimates over the north-east part of the study domain during the historical (Fig. S3) and full simulation (Fig. S5) periods, whereas the higher values shift to the south-east during the future period (Fig. S4).

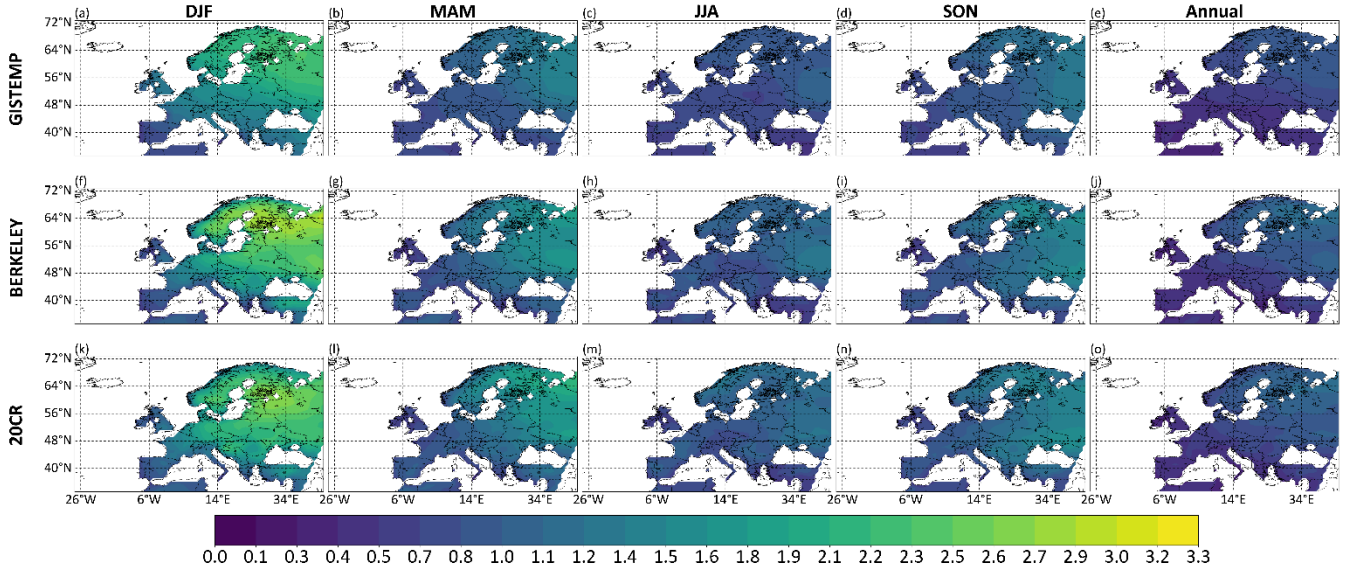

Figure 2: Seasonal and annual mean near-surface air temperature ICV estimates from the observational datasets (GISTEMP, Berkeley, and 20CR) data after the removal of components attributable to external forcings.

https://doi.org/10.5194/egusphere-2026-1341
Preprint. Discussion started: 13 April 2026

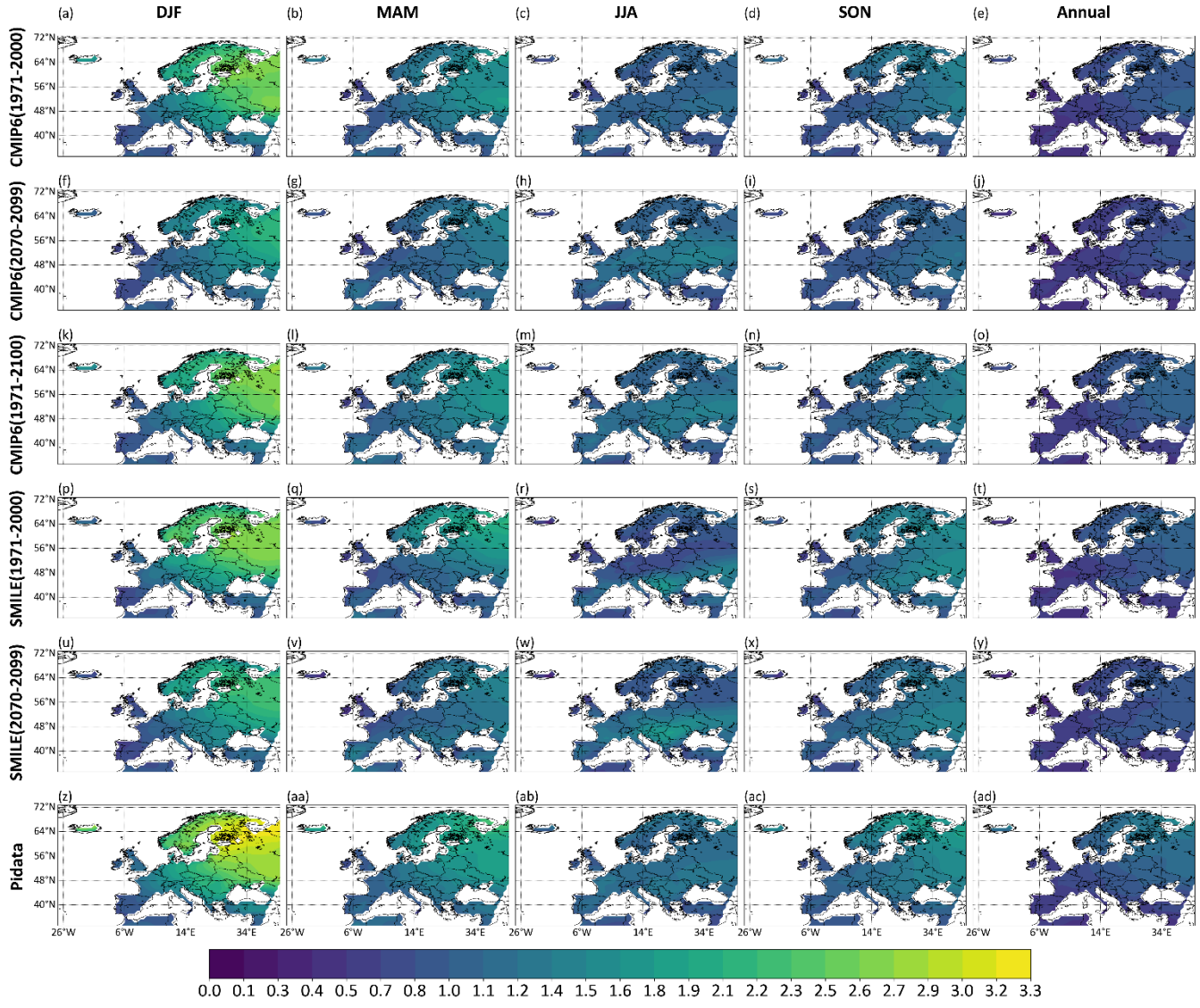

Figure 3: The same as Fig. 2, but for (a-o) multimodel mean of CMIP6 data, (p-y) SMILE data, and (z-ad) multimodel mean of Pidata. The columns represent individual seasons.

4.2 Spatial distribution of ICV estimates

The comparison of ICV estimates averaged over the four regions (Figs. 4-9) reveals several patterns. Firstly, by focusing on the methods, Pidata provide the highest estimates compared to the other approaches, except during JJA in all regions and in MAM over the CEU and the WCE (Figs. 4-9). This is evident in the values of Pidata ENSMEAN, which exceed all results from HS09, SMILEs, and observational data. Looking at individual models, the Pidata simulations of EC-Earth models have the highest ICV values (up to more than 2.0 °C during DJF and MAM over the NEU) (Fig. 5 and 6), except for JJA, in which

https://doi.org/10.5194/egusphere-2026-1341
Preprint. Discussion started: 13 April 2026

the highest ICV estimates are displayed by some of the historical and scenario CMIP6 simulations, especially by BCC-CSM2-MR, CMCC-CM2-SR5, EC-Earth3-Veg, and MPI-ESM1-LR. (Figs. 4-8). The ICV estimates based on the scenario simulations from HS09 and SMILE are lower than their historical period counterparts, except for JJA. This can be perceived through the values of ENSMEAN from Fig. 4-8 and the boxplot ranges in Fig. 9. In most cases, the lowest ICV estimates are displayed by some models from the scenario simulations based on HS09 (Fig. 9). Moreover, there is a marked difference between the estimates of historical and scenario simulations based on the HS09 method (Fig. 9). However, the differences between scenario and historical ICV estimates from SMILE simulations are quite small over most regions during all the time scales, except for DJF and JJA (Figs. 4-9). Among the observational data, GISTEMP shows the lowest ICV estimates, while Berkeley and 20CR display similar estimates for most of the cases. In general, despite the differences between the methods, there is good agreement between the modeled datasets and the observational ones. However, it is noticed that most of the modeled datasets display noticeably higher ICV estimates than the observational ones during JJA over all the regions, except the NEU. During DJF, while noticeably high ICV estimates are displayed for Pidata over NEU, the scenario simulations based on the HS09 method exhibit the lowest estimates over almost all the regions. Besides, the ENSMEAN estimate based on the HS09 method for historical simulations shows the best agreement with the observational-based estimates (Fig. 9). Overall, by comparing with the ENSMEAN, Pidata generally show the highest ICV estimates (except in JJA), while GISTEMP displays the lowest values (except in DJF).

Next, looking at different time scales through the boxplot visualization (Fig. 9), we can see that the annual ICV estimates are generally lower than for individual seasons (ranging from the lowest values between 0.4 °C and 0.7 °C over the MED to 0.5°C - 1.2 °C over the NEU). Moreover, the annual ICV estimates differ less than seasonal values between individual methods in each region. In the case of DJF, the differences between the methods are mostly higher than in other seasons, and the multi-model spread within the Pidata and HS09 methods is larger (Fig. 9). The highest inter-method variability is found over the NEU, with values ranging between 1.0 °C and 2.6 °C. The MAM ICV estimates are then lower, with its highest values from 0.8 °C to 2.0 °C over NEU. The JJA estimates are even lower than MAM, with its highest estimates ranging between 0.7 °C and 1.7 °C. SON displays similarly low seasonal ICV estimates, with its highest values between 0.7 °C and 1.5 °C over the WCE. The annual, JJA, and SON ICV estimates display better agreement among the methods since smaller differences between the ENSMEAN values of Pidata and HS09 for all time periods (noted as black dots in Fig. 9) are found compared to DJF. Overall, the annual ICV estimates show the lowest multi-model spread and differences between the methods, while the highest ICV is found during winter (DJF); the estimates then decrease from spring (MAM) until autumn (SON).

Finally, based on regional comparison, the MED region shows the lowest ICV magnitudes (ranging from 0.4 °C to 0.7°C for annual and 0.6 °C to 1.3°C for seasonal timescales) and the smallest data spreads and differences between the methods compared to the rest of the regions (Fig. 9). On the other hand, the NEU region exhibits the largest inter-method differences (except in JJA), especially during DJF (Fig. 9). Its annual ICV estimates range from 0.5 °C to 1.2 °C and the seasonal one from 0.5 °C - 2.6 °C. Then, it is followed by the WCE region, which displays the annual ICV estimates between 0.5 °C and 1.2°C and the seasonal values between 0.7 °C and 2.5 °C. Lastly, the CEU region displays slightly lower ICV

https://doi.org/10.5194/egusphere-2026-1341
Preprint. Discussion started: 13 April 2026

estimates and spreads than WCE. Its annual ICV estimates range from 0.4 °C to 1.0 °C, and its seasonal values range from 0.6 °C to 2.3 °C. Overall, the largest inter-method differences and the highest ICV estimates are found in the NEU region, where some of the Pidata models, such as BCC-CSM2-MR, EC-Earth3, and CNRM, show remarkably high estimates. It is then followed by WCE, CEU, and MED regions. In other words, better agreement between the methods is found over the MED than the rest of the regions. Also, the multi-model spread is the smallest over the MED.

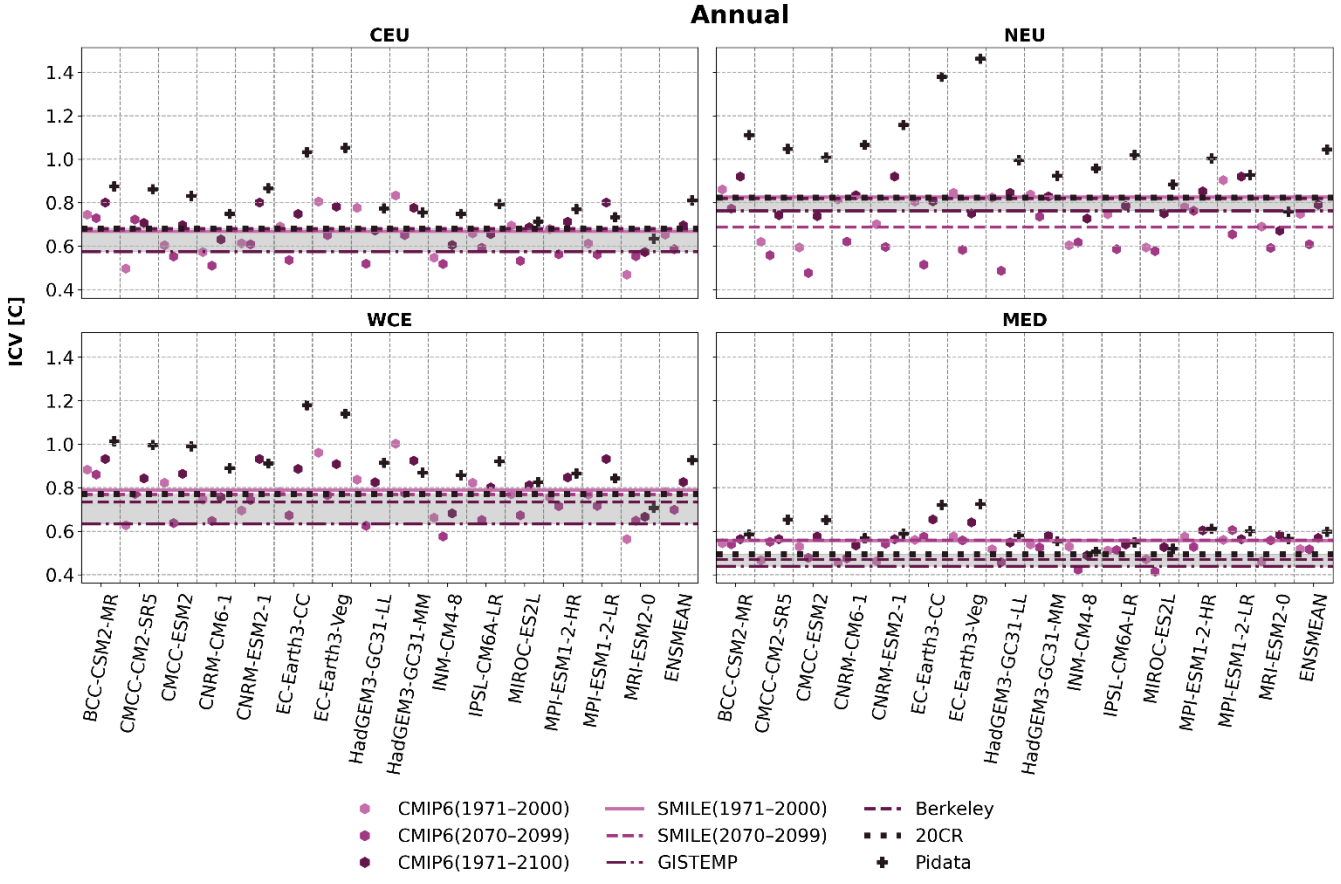

Figure 4: Regional mean of annual ICV based on Preindustrial control (Pidata), CMIP6 simulation, SMILE of MPI-ESM, and the observational data (GISTEMP, Berkeley, and 20CR). The shaded areas pertain to the differences between the three observational data sets.

https://doi.org/10.5194/egusphere-2026-1341
Preprint. Discussion started: 13 April 2026

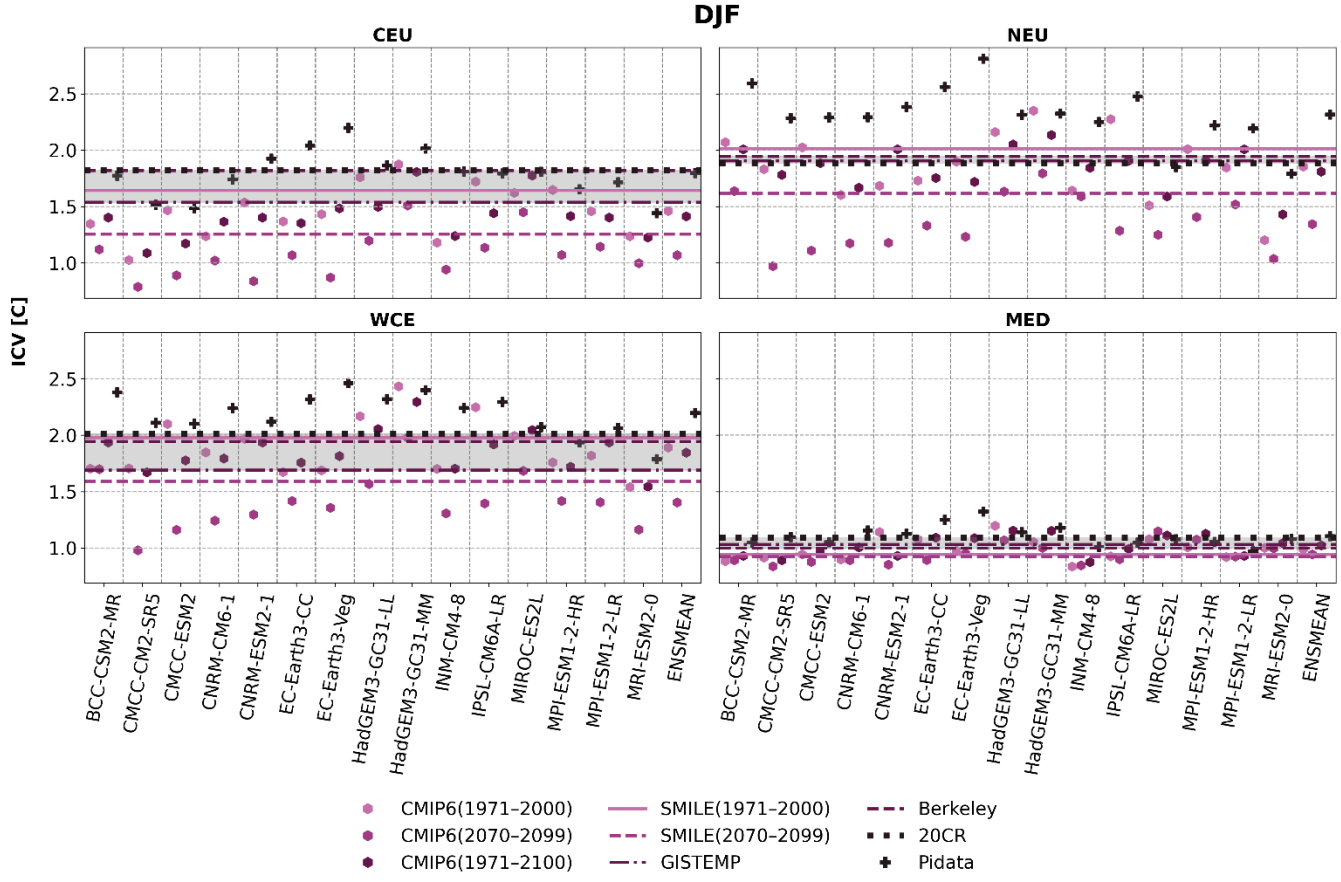

Figure 5: Same as Fig. 4 but for DJF seasonal mean.

https://doi.org/10.5194/egusphere-2026-1341
Preprint. Discussion started: 13 April 2026

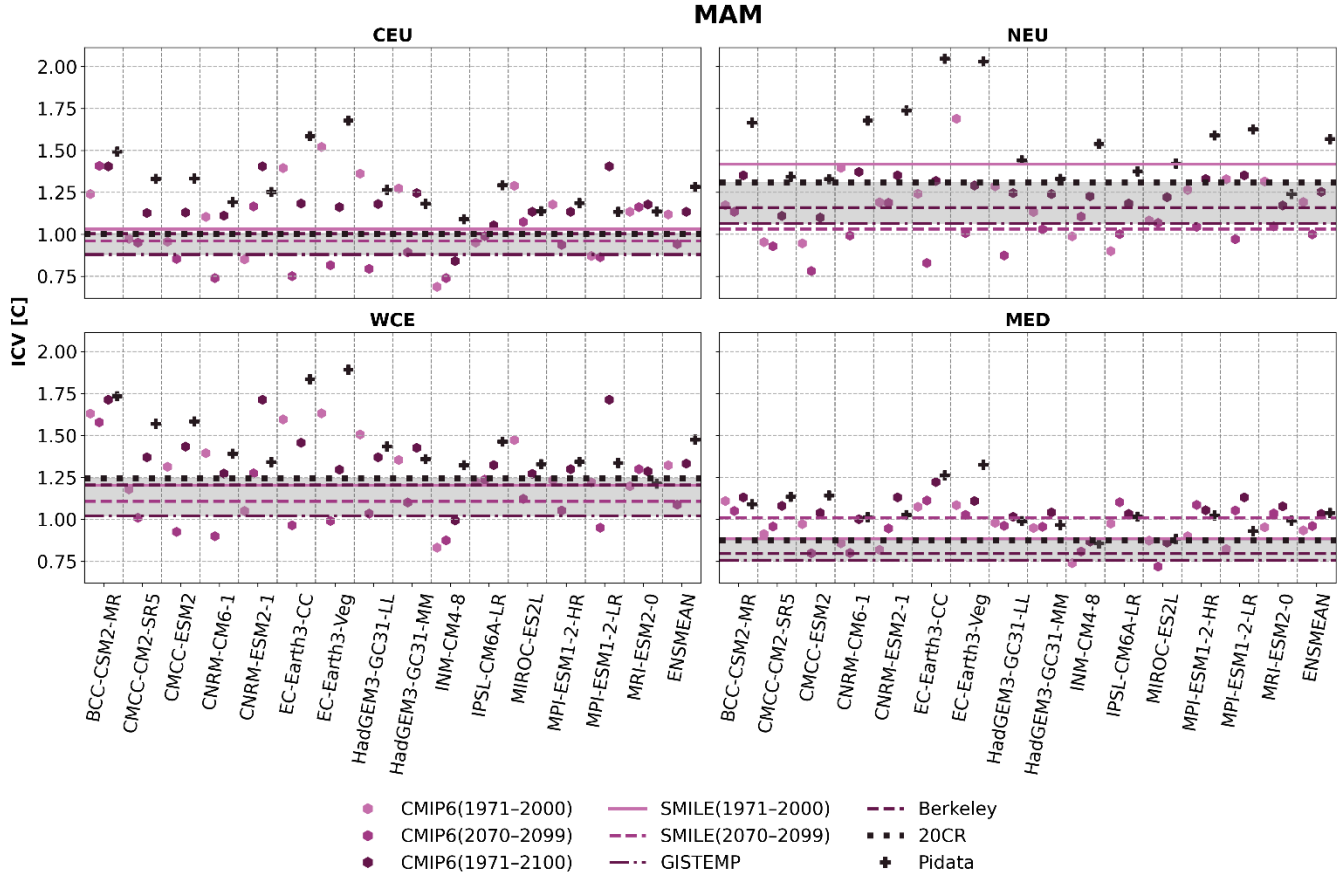

Figure 6: Same as Fig. 4 but for MAM seasonal mean.

https://doi.org/10.5194/egusphere-2026-1341
Preprint. Discussion started: 13 April 2026

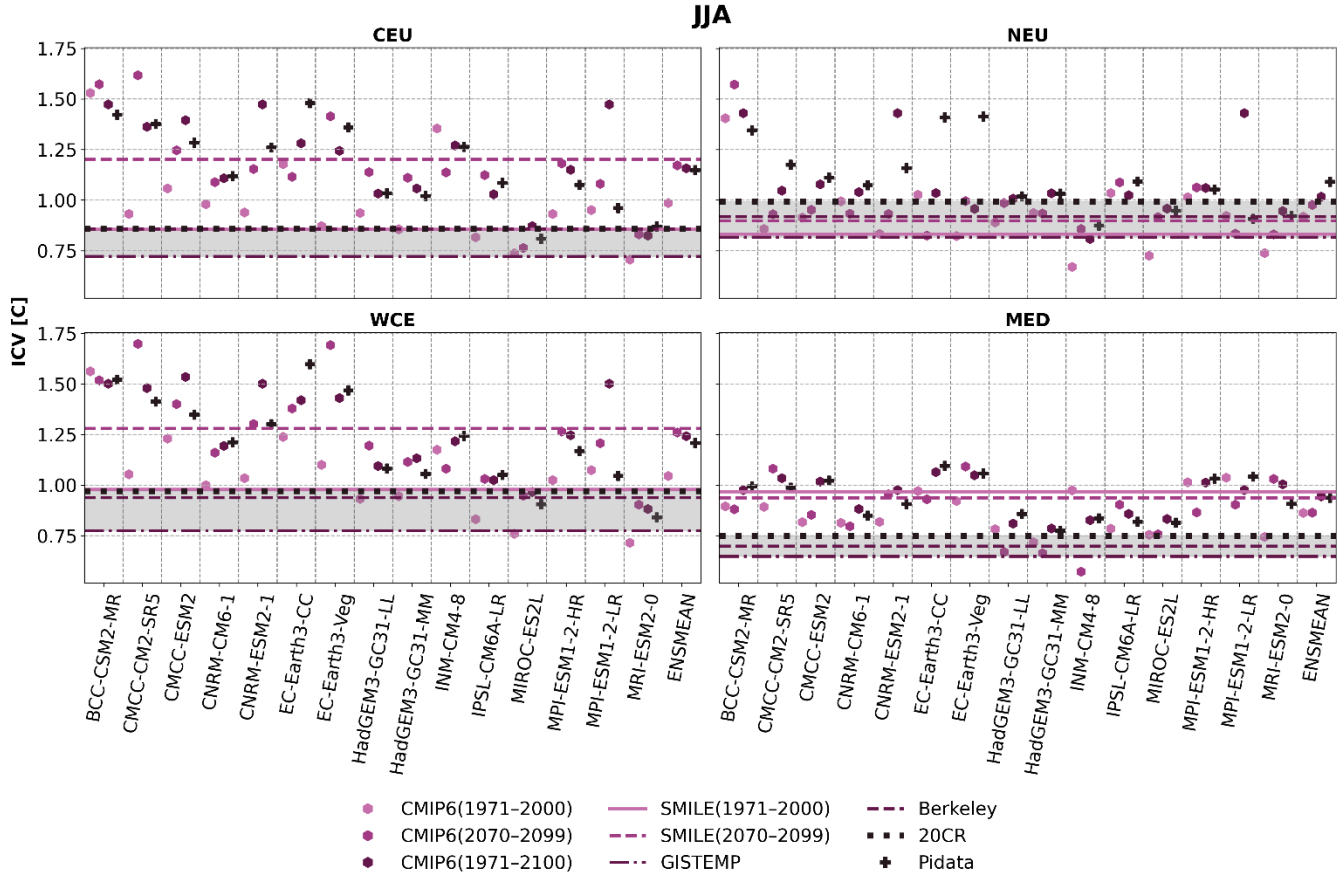

Figure 7: Same as Fig. 4 but for JJA seasonal mean.

https://doi.org/10.5194/egusphere-2026-1341
Preprint. Discussion started: 13 April 2026

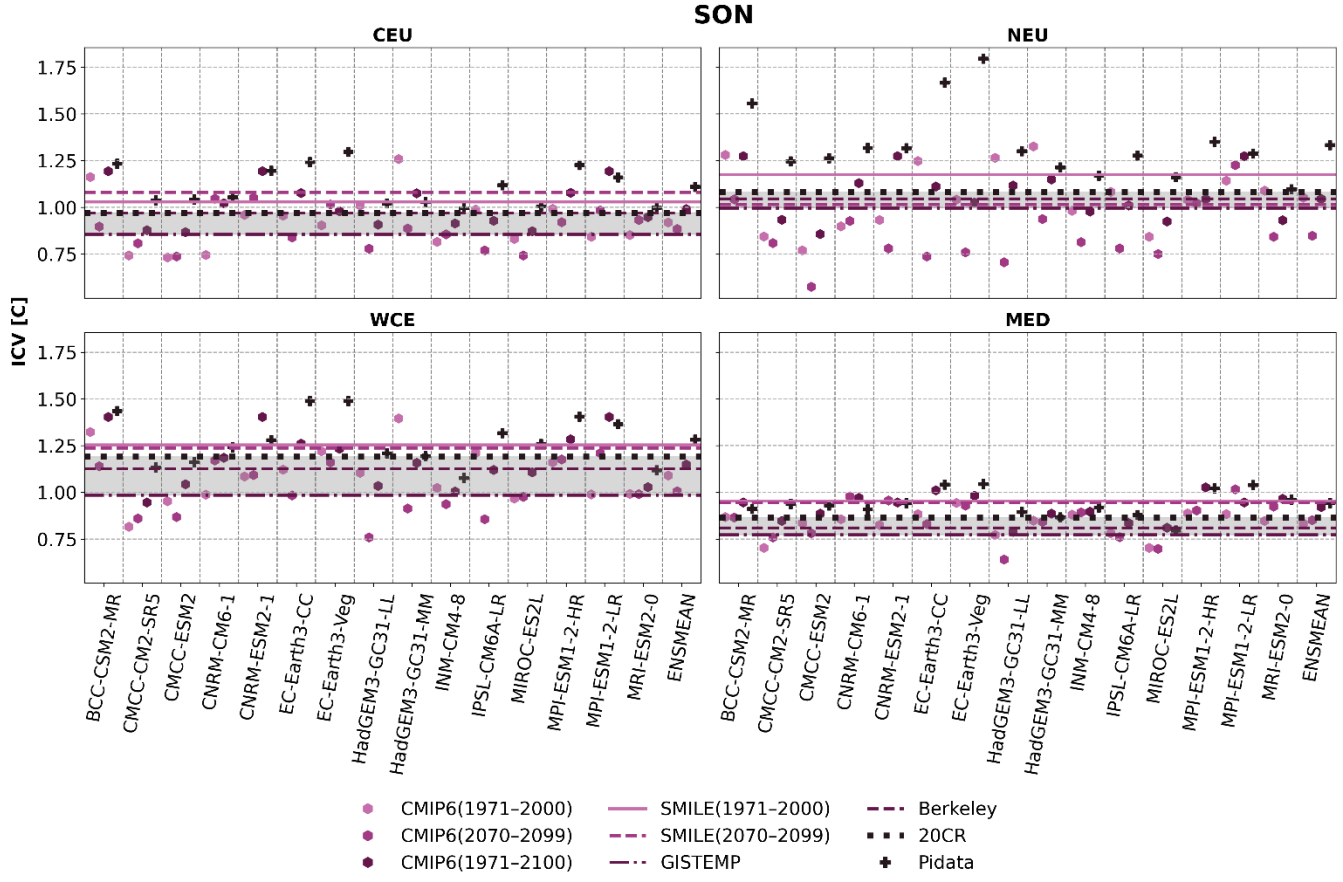

Figure 8: Same as Fig. 4 but for SON seasonal mean.

https://doi.org/10.5194/egusphere-2026-1341
Preprint. Discussion started: 13 April 2026

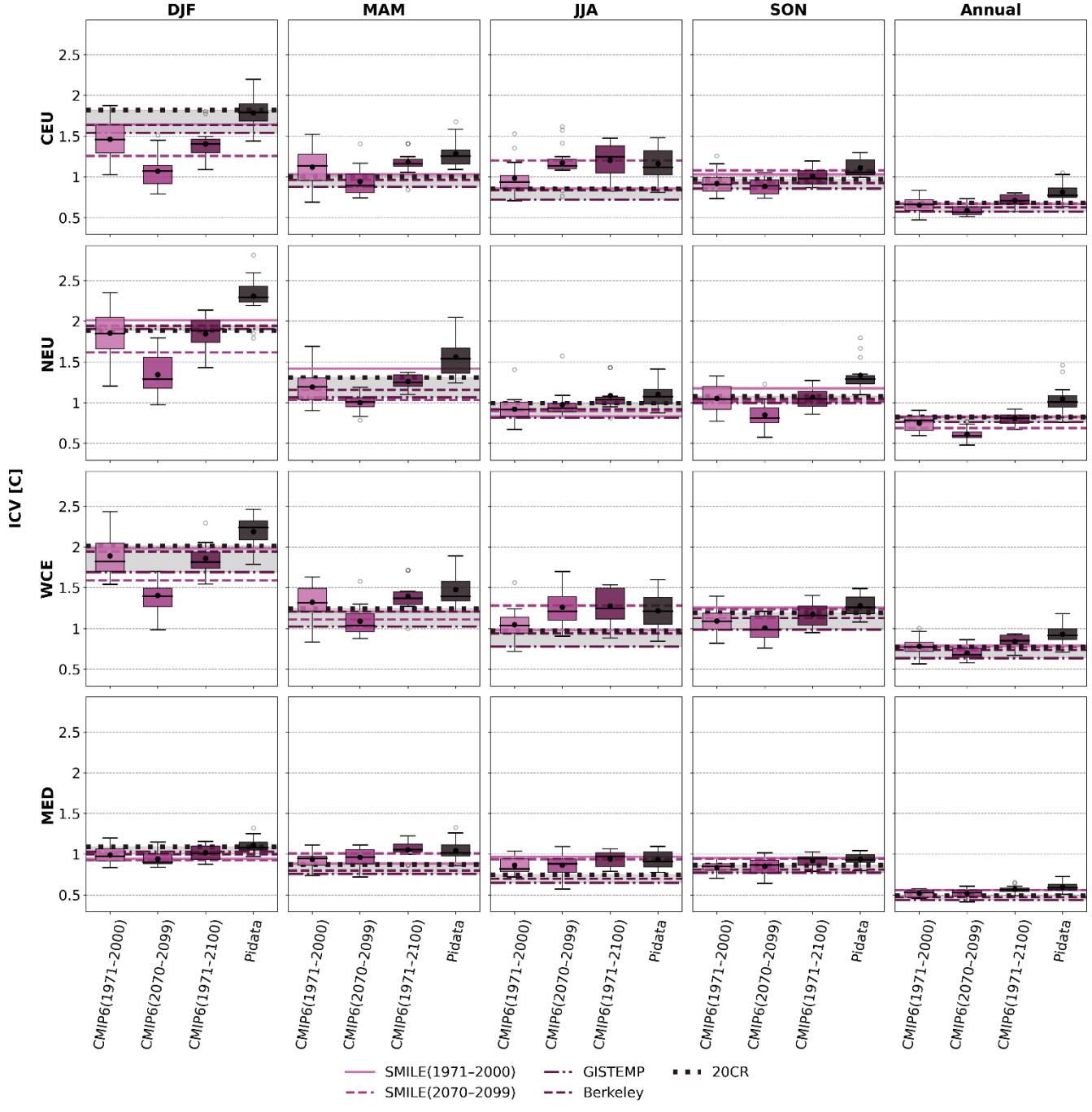

Figure 9: Seasonal and annual ICV estimates over each subregion. Boxplots show the results for the 15 models from CMIP6 and Pidata, with the dots displaying the ensemble mean value (ENSMEAN). The lines correspond to SMILE and observational results. The shaded areas pertain to the differences between the three observational data sets.

https://doi.org/10.5194/egusphere-2026-1341
Preprint. Discussion started: 13 April 2026

5 Discussion and conclusions

First, let us discuss the spatial distribution of the ICV estimates. Overall, the ICV across the European region decreases from north-east to south-west in both the annual and seasonal analyses, except during JJA, when the highest ICV magnitudes moved southward (Figs. 2, 3). Considering the regional means, the largest values are found especially over the NEU region, while the smallest are over the MED (Fig. 4-9). This general pattern of higher ICV in higher latitudes than in lower latitudes is consistent with previous studies by Deser et al. (2010) and Hyun et al. (2017). They used the same method as we did for the SMILE case, calculating anomalies for each member relative to their ensemble mean before computing the standard deviation across all members. The standard deviation was then defined as the final ICV estimate. Even though they used different models, Hyun et al. (2017) used the 30 members of CESM large ensemble, and Deser et al. (2010) used the 40 members of CCSM3; their findings are comparable. Deser et al. (2010) found that the internal atmospheric variability shapes a dominant pattern of the extra-tropical sea-level pressure, which subsequently drives the internal variability of extra-tropical temperature. They also showed that the ICV is larger than the model uncertainty over high latitude regions. Moreover, Hyun et al. (2017) suggested that the high ICV estimates over higher latitudes could be closely linked to the varied topography from middle to high latitudes and the south-north temperature gradient, coupled with a large thermal difference between land and ocean. While this general pattern of north-to-south decrease in ICV has been described previously on a global scale, our results demonstrate that internal variability over Europe is not spatially uniform and shows a pronounced decrease from northeastern Europe toward the southwestern and Mediterranean regions.

Comparing the ICV estimates for different seasons, throughout all the methods, our results show that DJF displays the largest ICV estimates compared to the annual time scale and the rest of the individual seasons. Likewise, Deser et al. (2010) also described the prominence of the highest temperature variability during the winter season through the computation of standard deviations and trend standard deviations by using several datasets.

The main contribution of our study is the comparison of ICV estimates based on different methods and datasets. Each approach is based on different assumptions, and the results differ in notable ways. Most of the methods have previously been used to estimate ICV magnitude, except HS09. The HS09 method has so far been used to assess only the relative importance of ICV uncertainty compared to structural and scenario uncertainties in climate change projections (Yip et al., 2011; Lehner et al., 2020; Zhang et al., 2023). To our knowledge, our study is the first application of the HS09 method for assessing the absolute magnitude of ICV estimates.

Pidata estimates are based on long time series, so they are robust in this sense, and we expected Pidata results to yield larger ICV estimates than HS09 based on CMIP6 data. The results confirm our expectations in most cases. Especially, the control simulations from BCC-CSM2-MR, EC-Earth3, and CNRM show notably high values, particularly over the extreme north of the study area. Parsons et al. (2020) concluded that these three models displayed unrealistically large estimates of internal interdecadal variability in comparison to the rest of the CMIP6 preindustrial control simulations. However, they reported that these models, similarly to most CMIP6 models, reproduce values similar to those from instrumental data when

https://doi.org/10.5194/egusphere-2026-1341
Preprint. Discussion started: 13 April 2026

driven by observed transient forcings from the industrial period (i.e., historical simulations). This corresponds well with our findings since the ICV estimates based on the HS09 method for all historical CMIP6 simulations (including the three above-mentioned models) generate better agreement with the observational data (Fig. 4-9) than their Pidata estimates. There seems to be no clear relationship between the model horizontal resolution and ICV estimates (not shown).

It is a fact that Pidata represent preindustrial climatic conditions, while the other model simulations used here, as well as observational data, are already influenced by the anthropogenic factors. However, the linear regression model applied to observational data cannot capture the changes in the variance of the temperature distribution that might have occurred during the 20th century. So, the observational data-based approach assumes that the ICV does not change as the result of anthropogenic forcings during the 20th century. The potential anthropogenic influence on ICV is here studied using the HS09 and SMILE approaches, comparing the historical and scenario simulations.

Looking at the ICV estimates based on historical and scenario simulations, we found that the historical CMIP6 HS09-based and SMILE simulations provide generally higher estimates of ICV than their scenario period counterparts, except for JJA. This could be related to what Hyun et al. (2017) found concerning the decrease of the ICV in the future climate due to the decrease of sea ice in the Arctic region between 70° and 90° N, which they identified as the primary source of ICV reduction all over the globe. Similarly, many papers have found a decrease in the future temperature variance over the extratropical regions, especially during the winter, using different methods and datasets, such as SMILEs (Olonscheck et al., 2021; Blanusa et al., 2023), observations (Screen, 2014), and CMIP models (Thompson et al., 2015; LaJoie and DelSole, 2016). One potential explanation for this feature, especially in winter, is that day-to-day temperature variability is strongly linked to synoptic-scale weather systems, and that, under global warming, their frequency is expected to decrease (e.g., Robeson, 2002; Cavanaugh and Shen, 2014). On the other hand, we must note that the scenario simulations we use for ICV estimates are limited, i.e., a relatively short time period in the case of CMIP6 (in comparison to Pidata), and only one model for SMILE. Therefore, the decrease of ICV estimated here for scenario simulations might be smaller; the ICV experienced in the future might be slightly higher than described in our study.

The large ensemble MPI-ESM provides a large sample of data, but it is based on only one model. The MPI-ESM SMILE during historical simulations show ICV estimates fairly in the middle of the values from all other methods. Thompson et al. (2015) concluded that CCSM3 preindustrial control simulations are sufficient to represent the ICV obtained from their SMILE with 40 members. However, in our present study, we cannot confirm that Pidata and MPI-ESM SMILE exhibit comparable ICV estimates in all cases. We only found that the ICV estimates based on the historical MPI-ESM SMILE are more comparable to the ICV estimates based on MPI-ESM1-2-LR from Pidata in many cases (except over the NEU region) than its scenario simulations. The difference between our findings might be related to the fact that our SMILE and Pidata model (MPI-ESM) is different than their model (CCSM3), and also, our MPI-ESM Pidata model is from the newer CMIP6 version, while our MPI-ESM SMILE is from CMIP5. Further, we found out that Pidata display higher ICV magnitudes in most cases, but this could be different if we were able to compare the same model between SMILE and Pidata. In our case,

https://doi.org/10.5194/egusphere-2026-1341
Preprint. Discussion started: 13 April 2026

only the MPI-ESM model was used for SMILE, since it provided the largest ensemble of individual simulations (100 members).

Concerning the observational-based estimates, they rely on real-world data, unlike the other methods, which use model simulations. However, there is still observational uncertainty. GISTEMP shows the lowest ICV estimates compared to the other observational data, and also lower values than the SMILEs and the ENSMEAN from HS09 and Pidata. The lower ICV estimates displayed by GISTEMP might be connected to its low resolution and probably to the number of stations considered over our study domain. In general, there are 6964 unique stations across the European domain, but many temperature stations are excluded due to insufficient records (Menne et al., 2012a).e In the case of the 20CR reanalysis, only surface air pressure is assimilated from station data, but other variables, including air temperature, are the output from the underlying model (Slivinski et al., 2019). Berkeley Earth used unique stations with approximately 39,000 records (far more numerous than GISTEMP (Cowtan et al., 2015)). Given that the 20CR and Berkeley station data are fundamentally different types of datasets (reanalysis and gridded station data, respectively), the fact that they display comparable ICV estimates suggests that the findings are robust.

To conclude, the ICV estimates decrease over the annual cycle from winter to autumn and spatially from north-eastern to south-western Europe. Pidata ENSMEAN exhibits the highest ICV estimates for almost all the seasonal and annual scales. The ICV estimates of historical simulations from both the SMILE MPI-ESM method and the ENSMEAN of the CMIP6 HS09-based method are comparable to the observational-based results. The higher ICV estimates from historical simulations compared to those from scenario simulations in both CMIP6 HS09-based and large ensemble simulations provide insight into how the ICV changes under externally forced climate change, revealing that it decreases under global warming. Even though the ICV estimates are projected to decrease, their spatial patterns remain unchanged in the scenario simulations. Interestingly, the observational-based estimates fall within the results from preindustrial and historical model simulations. Our main goal is to compare different methods of ICV estimation that could potentially be used as benchmarks for assessing regional climate simulations over Europe. Pidata have traditionally been used for this purpose, specifically in studies concentrating on global climate simulations (Olonschek and Notz, 2017). Our results imply that the estimate based on the ensemble mean value of pre-industrial control simulations (denoted here as Pidata ENSMEAN) encompasses the range of the other methods. An advantage of Pidata is that external forcings do not influence them. The externally forced climate change inevitably influences ICV estimates; as discussed above, an ICV decrease has been projected for warmer climates. So, when the focus is on future climate simulations, the estimates involving scenario simulations should be used, as they already account for the influence of anthropogenic forcings on ICV. Regarding the ICV estimates from the observational data, their advantage lies in considering climate history, free of modelling uncertainty. Historical simulations from CMIP6 and SMILE also include the influence of historical climate change and yield comparable ICV estimates to the observational data. The ICV estimate based on the HS09 method for the whole analysis period (1971-2099) could be of particular interest, as it combines both historical and scenario forcings. Its ENSMEAN estimates represent intermediate values compared with the other ICV estimate presented here.

https://doi.org/10.5194/egusphere-2026-1341
Preprint. Discussion started: 13 April 2026

Code and data availability

Computation codes are available on request from the main author, Herijaona Hani-Roge Hundilida Randriatsara. GISTEMP dataset is freely available at https://psl.noaa.gov/data/gridded/data.gistemp.html. The CHIRPS v2.0 data is available at https://psl.noaa.gov/data/gridded/data.20thC_ReanV3.html. Berkeley is available at https://berkeleyearth.org/data/. CMIP6 datasets are https://esgf-metagrid.cloud.dkrz.de/search/cmip6-dkrz/ and SMILE MPI-ESM is available at https://rda.ucar.edu/datasets/d651014/dataaccess/.

The outputs data sets can be accessed through the reference Randriatsara et al. (2026b).

Author contributions

H.H-R.H.R.: Conceptualization, data curation, formal analysis, data analysis, methodology, original draft writing. E.H.: Data analysis, conceptualization, methodology, project administration, review and editing, supervision, funding acquisition, validation. J.M.: Data analysis, methodology, review and editing.

Competing interests

No convection-permitting conflict of interest amongst the authors.

Disclaimer

Publisher's note: Copernicus Publications remains neutral with regard to jurisdictional claims made in the text, published maps, institutional affiliations, or any other geographical representation in this paper. While Copernicus Publications makes every effort to include appropriate place names, the final responsibility lies with the authors. Views expressed in the text are those of the authors and do not necessarily reflect the views of the publisher.

Acknowledgements

We acknowledge the World Climate Research Programme (WCRP), which, through its Working Group on Coupled Modelling, coordinated and promoted CMIP6; we thank the climate modelling groups for producing and making available their model output, including the SMILE (MPI-ESM) and preindustrial control simulations, and the Earth System Grid Federation (ESGF) for archiving the data and providing access. We also acknowledge Berkeley Earth for providing the global surface temperature dataset (Rohde et al., 2020) with their reference www.berkeleyearth.org for access. We acknowledge the NASA Goddard Institute for Space Studies (GISS) GISTEMP team for the surface temperature analysis (GISTEMP v4) and note that these data were accessed at https://data.giss.nasa.gov/gistemp/ on [28/11/2025]. For the 20th Century Reanalysis Version 3 dataset,

https://doi.org/10.5194/egusphere-2026-1341
Preprint. Discussion started: 13 April 2026

we acknowledge support provided by the U.S. Department of Energy Office of Science Biological and Environmental Research (BER), the NOAA Climate Program Office, and the NOAA Physical Sciences Laboratory (PSL), and we cite Slivinski et al. (2019) where appropriate.

Financial support

This research has been supported by the project nr. GA25-40615855S "Internal climate variability over Europe" funded by the Czech Science Foundation and the Johannes Amos Comenius Programme (OP JAC), project No. CZ.02.01.01/00/22_008/0004605, Natural and anthropogenic georisks.

References

Abramowitz, G., Herger, N., Gutmann, E., Hammerling, D., Knutti, R., Leduc, M., Lorenz, R., Pincus, R., and Schmidt, G. A.: Model dependence in multi-model climate ensembles: weighting, sub-selection and out-of-sample testing, Earth Syst. Dyn., 10, 91–105, https://doi.org/10.5194/esd-10-91-2019, 2019.

Bakker, P., Goosse, H., and Roche, D. M.: Internal climate variability and spatial temperature correlations during the past 2000 years. Clim. Past, 18, 2523–2544, https://doi.org/10.5194/cp-18-2523-2022, 2022.

Beobide-Arsuaga, G., Suarez-Gutierrez, L., Barkhordarian, A., Olonscheck, D., and Baehr, J.: Increasing central and northern European summer heatwave intensity due to forced changes in internal variability, Nat. Commun., 16, 9485, https://doi.org/10.1038/s41467-025-65392-w, 2025.

Bittner, M., Schmidt, H., Timmreck, C., and Sienz, F.: Using a large ensemble of simulations to assess the Northern Hemisphere polar vortex response to tropical volcanic eruptions, Geophys. Res. Lett., 43, 10,893–10,902, https://doi.org/10.1002/2016GL070851, 2016.

Blanusa, M. L., López-Zurita, C. J., and Rasp, S.: Internal variability plays a dominant role in global climate projections of temperature and precipitation extremes, Clim. Dyn., 61, 1931–1945, https://doi.org/10.1007/s00382-023-06664-3, 2023.

Cai, W., Borlace, S., Lengaigne, M., van Rensch, P., Collins, M., Vecchi, G., Timmermann, A., Santoso, A., McPhaden, M. J., Wu, L., England, M. H., Wang, G., Guilyardi, E., and Jin, F.-F.: ENSO and greenhouse warming: changes in variability and teleconnections, Nat. Clim. Change, 5, 849–858, https://doi.org/10.1038/nclimate2743, 2015.

Cavanaugh, N. R. and Shen, S. S. P.: Northern Hemisphere winter storm track changes during the twentieth century simulated by multiple reanalyses, Clim. Dyn., 43, 539–555, https://doi.org/10.1007/s00382-013-1951-7, 2014.

Chen, J., Li, X., Martel, J., Brissette, F. P., Zhang, X. J., and Frei, A.: Relative importance of internal climate variability versus anthropogenic climate change in global climate change, J. Climate, 34, 465–478, https://doi.org/10.1175/JCLI-D-20-0424.1, 2021.

https://doi.org/10.5194/egusphere-2026-1341
Preprint. Discussion started: 13 April 2026

Collins, M., An, S.-I., Cai, W., Ganachaud, A., Guilyardi, E., Jin, F.-F., Jochum, M., Lengaigne, M., Power, S., Timmermann, A., Vecchi, G., and Wittenberg, A.: The impact of global warming on the tropical Pacific Ocean and El Niño, Nat. Geosci., 3, 391–397, https://doi.org/10.1038/ngeo868, 2010.

Cowtan, K. and National Center for Atmospheric Research Staff (eds.): The Climate Data Guide: Global surface temperatures: BEST: Berkeley Earth Surface Temperatures, available at: https://climatedataguide.ucar.edu/climate-data/global-surface-temperatures-best-berkeley-earth-surface-temperatures, last modified: 11 December 2025, last access: 11 February 2026.

Deser, C. and Phillips, A. S.: A range of outcomes: the combined effects of internal variability and anthropogenic forcing on regional climate trends over Europe, Nonlin. Processes Geophys., 30, 63–84, https://doi.org/10.5194/npg-30-63-2023, 2023.

Deser, C., Phillips, A. S., Alexander, M. A., and Smoliak, B. V.: Projecting North American climate over the next 50 years: uncertainty due to internal variability, J. Climate, 27, 2271–2296, https://doi.org/10.1175/JCLI-D-13-00451.1, 2014.

Deser, C., Phillips, A., Bourdette, V., and Teng, H.: Uncertainty in climate change projections: the role of internal variability, Clim. Dyn., 38, 527–546, https://doi.org/10.1007/s00382-010-0977-x, 2010.

Deser, C.: Certain uncertainty: the role of internal climate variability in projections of regional climate change and risk management, Earth's Future, 8, e2020EF001854, https://doi.org/10.1029/2020EF001854, 2020.

Dethloff, K., Rinke, A., Handorf, D., Weisheimer, A., and Dorn, W.: Nonlinear dynamics of the climate system, in: The Climate in Historical Times, edited by: Fischer, H., Kumke, T., Lohmann, G., Flöser, G., Miller, H., von Storch, H., and Negendank, J. F. W., Springer, Berlin, Heidelberg, 17–48, https://doi.org/10.1007/978-3-662-10313-5_2, 2007.

Evin, G., Ribes, A., and Corre, L.: Assessing CMIP6 uncertainties at global warming levels, Clim. Dyn., 62, 8057–8072, https://doi.org/10.1007/s00382-024-07323-x, 2024.

Eyring, V., Bony, S., Meehl, G. A., Senior, C. A., Stevens, B., Stouffer, R. J., and Taylor, K. E.: Overview of the Coupled Model Intercomparison Project Phase 6 (CMIP6) experimental design and organization, Geosci. Model Dev., 9, 1937–1958, https://doi.org/10.5194/gmd-9-1937-2016, 2016.

Ghil, M. and Lucarini, V.: The physics of climate variability and climate change, Rev. Mod. Phys., 92, 035002, https://doi.org/10.1103/RevModPhys.92.035002, 2020.

Gosling, S. N., McGregor, G. R., and Lowe, J. A.: The benefits of quantifying climate model uncertainty in climate change impacts assessment: an example with heat-related mortality change estimates, Climatic Change, 112, 217–231, https://doi.org/10.1007/s10584-011-0211-9, 2012.

Gupta, A. S., Jourdain, N. C., Brown, J. N., and Monselesan, D.: Climate drift in the CMIP5 models, J. Climate, 26, 8597–8615, https://doi.org/10.1175/JCLI-D-12-00521.1, 2013.

Haller, M., Brienen, S., Brauch, J., and Früh, B.: Projection simulation with COSMO-CLM5-0-16 version V2022.01 (Downscaling of MIROC-MIROC5 data for Germany with 3 km grid spacing), Deutscher Wetterdienst [data set], https://doi.org/10.5676/DWD/CPS_SCEN_V2022.01, 2022.

Hawkins, E. and Sutton, R.: The potential to narrow uncertainty in regional climate predictions, Bull. Am. Meteorol. Soc., 90, 1095–1108, https://doi.org/10.1175/2009BAMS2607.1, 2009.

https://doi.org/10.5194/egusphere-2026-1341
Preprint. Discussion started: 13 April 2026

Hedemann, C., Mauritsen, T., Jungclaus, J. H., and Marotzke, J.: The subtle origins of surface-warming hiatuses, Nat. Clim. Change, 7, 336–339, https://doi.org/10.1038/nclimate3274, 2017.

Hyun, S.-H., Yeh, S.-W., and Yoon, J.: Reduction of internal climate variability in surface temperature due to sea-ice loss since the mid-21st century, Int. J. Climatol., 37, 5211–5216, https://doi.org/10.1002/joc.5146, 2017

IPCC: Climate Change 2021: The Physical Science Basis, Contribution of Working Group I to the Sixth Assessment Report of the Intergovernmental Panel on Climate Change, Cambridge University Press, sections on internal variability and nonlinear climate-system coupling, https://doi.org/10.1017/9781009157896, 2021a.

IPCC: Climate Change 2021: The Physical Science Basis, Contribution of Working Group I to the Sixth Assessment Report of the Intergovernmental Panel on Climate Change, Cambridge University Press, sections on internal climate variability (ENSO, AMV, PDO) and intrinsic dynamical randomness, https://doi.org/10.1017/9781009157896, 2021b.

IPCC: Human influence on the climate system, in: Climate Change 2021: The Physical Science Basis, Contribution of Working Group I to the Sixth Assessment Report of the Intergovernmental Panel on Climate Change, edited by: Masson-Delmotte, V., Zhai, P., Pirani, A., Connors, S. L., Péan, C., Berger, S., Caud, N., Chen, Y., Goldfarb, L., Gomis, M. I., Huang, M., Leitzell, K., Lonnoy, E., Matthews, J. B. R., Maycock, T. K., Waterfield, T., Yelekçi, O., Yu, R., and Zhou, B., Cambridge University Press, Cambridge, UK and New York, NY, USA, 423–552, https://doi.org/10.1017/9781009157896.005, 2021c.

Iturbide, M., Gutiérrez, J. M., Alves, L. M., Bedia, J., Cerezo-Mota, R., Cimadevilla, E., Cofiño, A. S., Di Luca, A., Faria, S. H., Gorodetskaya, I. V., Hauser, M., Herrera, S., Hennessy, K., Hewitt, H. T., Jones, R. G., Krakovska, S., Manzanas, R., Martínez-Castro, D., Narisma, G. T., Nurhati, I. S., Pinto, I., Seneviratne, S. I., van den Hurk, B., and Vera, C. S.: An update of IPCC climate reference regions for subcontinental analysis of climate model data: definition and aggregated datasets, Earth Syst. Sci. Data, 12, 2959–2970, https://doi.org/10.5194/essd-12-2959-2020, 2020.

Jain, S., Scaife, A. A., Shepherd, T. G., Deser, C., Dunstone, N., Schmidt, G. A., Trenberth, K. E., and Turkington, T.: Importance of internal variability for climate model assessment, npj Clim. Atmos. Sci., 6, 68, https://doi.org/10.1038/s41612-023-00389-0, 2023.

Kay, J. E., Deser, C., Phillips, A., Mai, A., Hannay, C., Strand, G., Arblaster, J., Bates, S. C., Danabasoglu, G., Edwards, J., Holland, M., Kushner, P., Lamarque, J.-F., Lawrence, D., Lindsay, K., Middleton, A., Muñoz, E., Neale, R., Oleson, K., Polvani, L., and Vertenstein, M.: The Community Earth System Model (CESM) Large Ensemble Project: a community resource for studying climate change in the presence of internal climate variability, Bull. Am. Meteorol. Soc., 96, 1333–1349, https://doi.org/10.1175/BAMS-D-13-00255.1, 2015.

Knutti, R. and Sedláček, J.: Robustness and uncertainties in the new CMIP5 climate model projections, Nat. Clim. Change, 3, 369–373, https://doi.org/10.1038/nclimate1716, 2012.

Krishnamurthy, V.: Predictability of weather and climate, Earth Space Sci., 6, 1043–1056, https://doi.org/10.1029/2019EA000586, 2019.

LaJoie, E. and DelSole, T.: Changes in internal variability due to anthropogenic forcing: a new field significance test, J. Climate, 29, 5547–5560, https://doi.org/10.1175/JCLI-D-15-0718.1, 2016.

https://doi.org/10.5194/egusphere-2026-1341
Preprint. Discussion started: 13 April 2026

Lehner, F. and Deser, C.: The importance of internal variability for the uncertainty in climate change projections and decision-making, in: Uncertainty in Climate Change Research, edited by: Mearns, L. O., Forest, C. E., Fowler, H. J., Lempert, R., and Wilby, R. L., Springer, Cham, https://doi.org/10.1007/978-3-031-85542-9_17, 2025.

Lehner, F., Deser, C., and Sanderson, B. M.: Biased variability in climate models, J. Climate, 30, 6395–6411, https://doi.org/10.1175/JCLI-D-16-0033.1, 2017.

Lehner, F., Deser, C., Maher, N., Marotzke, J., Fischer, E. M., Brunner, L., Knutti, R., and Hawkins, E.: Partitioning climate projection uncertainty with multiple large ensembles and CMIP5/6, Earth Syst. Dynam., 11, 491–508, https://doi.org/10.5194/esd-11-491-2020, 2020.

Lenssen, N., Schmidt, G. A., Hendrickson, M., Jacobs, P., Menne, M. J., and Ruedy, R.: A NASA GISTEMPv4 observational uncertainty ensemble. Journal of Geophysical Research: Atmospheres, 129(17), e2023JD040179. https://doi.org/10.1029/2023JD040179, 2024.

Lorenz, E. N.: Deterministic nonperiodic flow, J. Atmos. Sci., 20, 130–141, https://doi.org/10.1175/1520-0469(1963)020<0130:DNF>2.0.CO;2, 1963.

Lorenz, E. N.: Predictability: a problem partly solved, in: Seminar on Predictability, ECMWF, Reading, UK, 1–18, 1996.

Maher, N., Lehner, F., and Marotzke, J.: Quantifying the role of internal variability in the temperature we expect to observe in the coming decades, Environ. Res. Lett., 15, 054014, https://doi.org/10.1088/1748-9326/ab7d02, 2020.

Maher, N., Milinski, S., and Ludwig, R.: Large ensemble climate model simulations: introduction, overview, and future prospects for utilising multiple types of large ensemble, Earth Syst. Dynam., 12, 401–418, https://doi.org/10.5194/esd-12-401-2021, 2021.

Maher, N., Milinski, S., Suarez-Gutierrez, L., Botzet, M., Dobrynin, M., Kornblueh, L., Kröger, J., Takano, Y., Ghosh, R., Hedemann, C., Li, C., Li, H., Manzini, E., Notz, D., Putrasahan, D., Boysen, L., Claussen, M., Ilyina, T., Olonscheck, D., Raddatz, T., Stevens, B., and Marotzke, J.: The Max Planck Institute Grand Ensemble: enabling the exploration of climate system variability, J. Adv. Model. Earth Syst., 11, 2050–2069, https://doi.org/10.1029/2019MS001639, 2019.

Mann, M. E., Steinman, B. A., Brouillette, D. J., Fernandez, A., and Miller, S. K.: On the estimation of internal climate variability during the preindustrial past millennium, Geophys. Res. Lett., 49, e2021GL096596, https://doi.org/10.1029/2021GL096596, 2022.

Martel, J., Mailhot, A., Brissette, F., and Caya, D.: Role of natural climate variability in the detection of anthropogenic climate change signal for mean and extreme precipitation at local and regional scales, J. Climate, 31, 4241–4263, https://doi.org/10.1175/JCLI-D-17-0282.1, 2018.

McWilliams, J. C.: Irreducible imprecision in atmospheric and oceanic simulations, Proc. Natl. Acad. Sci. USA, 104, 8709–8713, https://doi.org/10.1073/pnas.0702971104 (doi.org in Bing), 2007.

Menary, M. B., Kuhlbrodt, T., Ridley, J., Andrews, M. B., Dimdore-Miles, O. B., Deshayes, J., et al.: Preindustrial control simulations with HadGEM3-GC3.1 for CMIP6, J. Adv. Model. Earth Syst., 10, 3049–3075, https://doi.org/10.1029/2018MS001495, 2018.

https://doi.org/10.5194/egusphere-2026-1341
Preprint. Discussion started: 13 April 2026

Menne, M. J., Durre, I., Vose, R. S., Gleason, B. E., and Houston, T. G.: An overview of the Global Historical Climatology Network-Daily Database, J. Atmos. Oceanic Technol., 29, 897–910, https://doi.org/10.1175/JTECH-D-11-00103.1, 2012.

Mikšovský, J., Holtanová, E., and Pisoft, P.: Imprints of climate forcings in global gridded temperature data, Earth Syst. Dynam., 7, 231–249, https://doi.org/10.5194/esd-7-231-2016, 2016.

Newman, M., Alexander, M. A., Ault, T. R., Cobb, K. M., Deser, C., Di Lorenzo, E., Mantua, N., Miller, A. J., Minobe, S., Nakamura, H., Schneider, N., Vimont, D. J., Phillips, A. S., Scott, J. D., and Smith, C. A.: The Pacific Decadal Oscillation, revisited, J. Climate, 29, 4399–4427, https://doi.org/10.1175/JCLI-D-15-0508.1, 2016.

Olonscheck, D. and Notz, D.: Consistently estimating internal climate variability from climate model simulations, J. Climate, 30, 9555–9573, https://doi.org/10.1175/JCLI-D-16-0428.1, 2017.

Olonscheck, D., Schurer, A. P., Lücke, L., and Hegerl, G. C.: Large-scale emergence of regional changes in year-to-year temperature variability by the end of the 21st century, Nat. Commun., 12, 7237, https://doi.org/10.1038/s41467-021-27515-x, 2021.

Palmer, T. N.: A nonlinear dynamical perspective on climate prediction, J. Climate, 12, 575–591, https://doi.org/10.1175/1520-0442(1999)012<0575:ANDPOC>2.0.CO;2, 1999.

Parsons, L. A., Brennan, M. K., Wills, R. C. J., and Proistosescu, C.: Magnitudes and spatial patterns of interdecadal temperature variability in CMIP6, Geophys. Res. Lett., 47, e2019GL086588, https://doi.org/10.1029/2019GL086588, 2020.

Randriatsara, H. H.-R. H. and Holtanová, E.: Central European climate change from the convection permitting regional climate model perspective, [To be submitted], 2026a.

Randriatsara, H. H.-R. H., Holtanová, E., & Mikšovský, J.: Combining different views on internal climate variability of temperature over Europe [Data set]. Zenodo. https://doi.org/10.5281/zenodo.18924090, 2026b.

Rehfeld, K., Hébert, R., Lora, J. M., Lofverstrom, M., and Brierley, C. M.: Variability of surface climate in simulations of past and future, Earth Syst. Dynam., 11, 447–468, https://doi.org/10.5194/esd-11-447-2020, 2020.

Robeson, S. M.: Increasing winter temperature variability in the continental United States, Geophys. Res. Lett., 29, 1921, https://doi.org/10.1029/2002GL015341, 2002.

Rodgers, K. B., Lee, S.-S., Rosenbloom, N., Timmermann, A., Danabasoglu, G., Deser, C., Edwards, J., Kim, J.-E., Simpson, I. R., Stein, K., Stuecker, M. F., Yamaguchi, R., Bódai, T., Chung, E.-S., Huang, L., Kim, W. M., Lamarque, J.-F., Lombardozzi, D. L., Wieder, W. R., and Yeager, S. G.: Ubiquity of human-induced changes in climate variability, Earth Syst. Dynam., 12, 1393–1411, https://doi.org/10.5194/esd-12-1393-2021, 2021.

Rohde, R. A. and Hausfather, Z.: The Berkeley Earth Land/Ocean Temperature Record, Earth Syst. Sci. Data, 12, 3469–3479, https://doi.org/10.5194/essd-12-3469-2020, 2020.

Schwarzwald, K. and Lenssen, N.: The importance of internal climate variability in climate impact projections, Proc. Natl. Acad. Sci. USA, 119, e2208095119, https://doi.org/10.1073/pnas.2208095119, 2022.

Screen, J. A.: Arctic amplification decreases temperature variance in northern mid- to high-latitudes, Nat. Clim. Change, 4, 577–582, https://doi.org/10.1038/nclimate2268, 2014.

https://doi.org/10.5194/egusphere-2026-1341
Preprint. Discussion started: 13 April 2026

Shen, Z., Duan, A., Zhou, W., Peng, Y., and Li, J.: Reconciling roles of external forcing and internal variability in Arctic sea-ice change on different time scales, J. Climate, 37, 3577–3591, https://doi.org/10.1175/JCLI-D-23-0280.1, 2024.

Sippel, S., Meinshausen, N., Székely, E., Fischer, E. M., Pendergrass, A. G., Lehner, F., and Knutti, R.: Robust detection of forced warming in the presence of potentially large climate variability, Sci. Adv., 7, eabj3039, https://doi.org/10.1126/sciadv.abj3039, 2021.

Slivinski, L. C., Compo, G. P., Whitaker, J. S., Sardeshmukh, P. D., Giese, B. S., McColl, C., Allan, R., Yin, X., Vose, R., et al.: NOAA–CIRES–DOE Twentieth Century Reanalysis Version 3, Research Data Archive at the National Center for Atmospheric Research, Computational and Information Systems Laboratory, https://doi.org/10.5065/H93G-WS83, 2019.

Snyder, A., Prime, N., Tebaldi, C., and Dorheim, K.: Uncertainty-informed selection of CMIP6 Earth system model subsets for use in multisectoral and impact models, Earth Syst. Dynam., 15, 1301–1318, https://doi.org/10.5194/esd-15-1301-2024, 2024.

Suárez-Gutiérrez, L., Li, C., Müller, W. A., and Marotzke, J.: Internal variability in European summer temperatures at 1.5 °C and 2 °C of global warming, Environ. Res. Lett., 13, 064026, https://doi.org/10.1088/1748-9326/aaba58, 2017.

Suárez-Gutiérrez, L., Milinski, S., and Maher, N.: Exploiting large ensembles for a better yet simpler climate model evaluation, Clim. Dyn., 57, 2557–2580, https://doi.org/10.1007/s00382-021-05821-w, 2018.

Thompson, D. W. J., Barnes, E. A., Deser, C., Foust, W. E., and Phillips, A. S.: Quantifying the role of internal climate variability in future climate trends, J. Climate, 28, 6443–6456, https://doi.org/10.1175/JCLI-D-14-00830.1, 2015.

Van Achter, G., Ponsoni, L., Massonnet, F., Fichefet, T., and Legat, V.: Brief communication: Arctic sea-ice thickness internal variability and its changes under historical and anthropogenic forcing, The Cryosphere, 14, 3479–3486, https://doi.org/10.5194/tc-14-3479-2020, 2020.

Werndl, C.: Initial-condition dependence and initial-condition uncertainty in climate science, Br. J. Philos. Sci., 70, 953–976, https://www.jstor.org/stable/26842362, 2019.

Yip, S., Ferro, C. A. T., Stephenson, D. B., and Hawkins, E.: A simple, coherent framework for partitioning uncertainty in climate predictions, J. Climate, 24, 4634–4643, https://doi.org/10.1175/2011JCLI4085.1, 2011.

Zappa, G., Bevacqua, E., and Shepherd, T. G.: Communicating potentially large but non-robust changes in multi-model projections of future climate, Int. J. Climatol., 41, 3657–3669, https://doi.org/10.1002/joc.7041, 2021.

Zhang, S., Zhou, Z., Peng, P., and Xu, C.: A new framework for estimating and decomposing the uncertainty of climate projections, J. Climate, 37, 365–384, https://doi.org/10.1175/JCLI-D-23-0064.1, 2023.